Nuclear Materials and Energy 18 (2019) 291–296

Contents lists available at ScienceDirect

Nuclear Materials and Energy

journal homepage: www.elsevier.com/locate/nme

Performance estimation of beryllium under ITER relevant transient thermal loads

B. Spilker*, J. Linke, Th. Loewenhoff, G. Pintsuk, M. Wirtz

Forschungszentrum Jülich GmbH, Institut für Energie- und Klimaforschung, 52425 Jülich, Germany

ARTICLE INFO

Keywords:
ITER
First wall
Plasma facing materials
Beryllium
Erosion
Transient thermal load
ELMs
Massive gas injections
Shattered pellet injections

ABSTRACT

The plasma facing first wall in ITER will be armored with beryllium. During operation, the armor has to sustain direct plasma contact during the start-up and ramp-down of the plasma. On top, transient thermal loads originating from a variety of plasma instabilities or mitigation systems are impacting the 8–10 mm thick beryllium tiles. In this work, possible armor thickness losses caused by the expected transient heat loads are reviewed. Applying conservative assumptions, vertical displacement events can cause locally a melt layer with a thickness of up to 3 mm. However, cracks after solidification/cool down are confined to the melt layer and the connection between melt layer and bulk remains strong. Radiative cooling mechanisms can be applied to significantly decrease the melt and evaporation layer thickness. To mitigate the critical damage potential of plasma disruptions, massive gas injections or shattered pellet injections can be deployed to transform the stored plasma energy into radiation, which implies a much more homogeneous distribution of energy to the plasma facing components. For a full power plasma discharge in ITER, these radiative loads can cause temperatures exceeding the melting temperature of beryllium. Experiments have demonstrated that a thickness of 340 μm at the entire first wall armor can be affected by these mechanisms over the lifetime of ITER. Edge localized modes with expected characteristics obtained by fluid model simulations caused fatigue cracks with a depth of up to 350 μm in experimental simulations. The critical heat flux factor F_{HF} above which inflicted damage accumulates with each subsequent pulse has been determined to be in the range of $F_{HF} \approx$ 9–12 MW m^{-2} s$^{0.5}$. The damage from thermal loads below this threshold saturates between 10^4 and 10^6 pulses. Neutron irradiation has a deteriorating effect on the thermomechanical properties of beryllium, which strongly influence its resistance against thermally induced damages. The rather low neutron fluence over the lifetime of ITER is expected to reduce the material strength and thermal conductivity by a few tens of percents. If the thickness losses are affected to a similar extent, a sufficient margin of armor thickness will remain. Overall, the damage imposed by radiative loads from massive gas injections or shattered pellet injections is expected to be the dominant force influencing the condition of the first wall armor, at least if all disruptions can be successfully mitigated and the number of vertical displacement events can be constrained to a few occurrences over the service time of ITER.

1. Introduction

Beryllium has been chosen as armor material for the plasma facing main chamber wall in ITER. This choice was driven by a variety of favorable characteristics of beryllium, namely its particularly advantageous plasma compatibility, remarkable thermal conductivity, and oxygen getter capability to ensure clean vacuum conditions. The first wall (FW) in ITER arguably represents one of the key components by covering about 620 m^2 of the inner main chamber surface area [1]. The stored plasma energy for a typical high performance plasma discharge will increase from 10 MJ in JET [2], the largest currently operational tokamak, to 350 MJ in ITER [3]. At the same time, the plasma facing surface area only increases by a factor of ~4 from JET to ITER. Taking these numbers into account, it becomes clear that the potential effect of transient plasma events on the plasma facing components is drastically enhanced in ITER. Although not in direct contact with the scrape-off layer between the start-up and ramp-down phases of the plasma discharge, the FW needs to withstand strong particle and thermal loads. Especially transient plasma events involve the potential to plastically deform or even melt the surface of the beryllium armor tiles.

The initial thickness of the beryllium tiles is 8–10 mm. Due to the thickness constraints originating from the thermal design, it is vital to estimate possible armor thickness losses due to erosion in the steady

* Corresponding author.
E-mail address: b.spilker@fz-juelich.de (B. Spilker).

https://doi.org/10.1016/j.nme.2018.12.026
Received 28 August 2018; Received in revised form 18 December 2018; Accepted 20 December 2018
Available online 22 January 2019

state operation and due to transient events. Calculations as well as experiments that examined the erosion of beryllium due to impurity ions and charge exchange neutrals are presented in [4–7]. It was ascertained that about 20–40 g of beryllium are eroded from the armor tiles per 400 s discharge duration. Thereby, the peak erosion rate was found to be in the order of 0.1 nm s^{-1}, which is in agreement with the extrapolation of experimental data obtained in the Joint European Torus (JET) [8]. As the most conservative assessment, 30,000 ITER discharges with the peak erosion rate add up to a total thickness loss of 1.2 mm. Considering the fact that a large fraction of these discharges are low energy discharges during the early operational phase of ITER, this upper limit for the erosion rate appears acceptable for the FW components.

Implications of the beryllium erosion for the divertor, mixed material formation, and possible co-deposition of fuel are discussed elsewhere [9–11]. This paper aims to review and discuss the performance and possible affected armor thickness of beryllium due to transient events, which will add to the steady state erosion losses. The structuring is as follows. Section 2 provides an overview about all kinds of transient thermal loads that are expected to affect the FW in ITER and possible armor thickness losses attributed to them. In Section 3, an overview of transient thermal loads with different absorbed power densities and pulse durations, which are combined and compared via the heat flux factor [12,13], is provided. For a comparison between transient thermal loads applied in different machines, the temporal pulse shape plays an important role, due to the fact that it affects the peak surface temperature and the material damage [14]. For the calculation of the heat flux factor in this work, a rectangular temporal pulse shape with the respective peak power density is assumed. In addition, a thorough discussion on the influence of the number of pulses on the development of damage/melting thresholds, oxidation effects, and the influence of neutron irradiation on the performance of beryllium is presented.

2. Transient loads at the first wall

The operation of a large scale fusion plasma is tied to the possible occurrence of strong transient thermal loads on the plasma facing components during different kinds of plasma instabilities. A schematic of how beryllium responds to the exposure to transient thermal loads depending on the absorbed energy density is provided in Fig. 1.

Since electron beam machines have proven to be an effective experimental testing method to investigate and to qualify materials under transient thermal loading [15–17], Fig. 1(a) depicts a typical scanning electron beam loading with 120 keV electrons in the JUDITH 1 facility [18]. Further established methods to experimentally test transient thermal loads with fusion relevant characteristics are quasi static plasma accelerators (QSPA) [19] and lasers [20]. In the following, different transient plasma events that are expected to play a role in ITER and the range of energy densities they can deposit on the FW are discussed one by one.

2.1. Vertical displacement events (VDEs)

If the control over the vertical position of the plasma is temporarily lost, the plasma facing components can suffer strong thermal loads from the resulting direct contact with plasma particle trajectories. For ITER, the expected energy density is in the order of 60 MJ m^{-2}, deposited over 100–500 ms, translating to 120–600 MWm^{-2} [21]. From all transient events discussed in this section, VDEs have the longest duration and the strongest potential to impact the interface between the beryllium tiles and the heat sink structure. VDEs, even on the lower end of the energy density spectrum, will certainly cause melting of the beryllium surface. At low energy densities, a homogeneous melt layer is formed on beryllium followed by cracking in the resolidified material. At an energy density of 40 MJ m^{-2}, the melt layer becomes unstable, melt is ejected, and the affected area forms a deep crater. The cracks that form in the resolidified material do not extend beyond the melt layer [22] and are oriented perpendicular to the loaded surface in all observed cases [23]. Calculations as well as further electron beam experiments have determined the maximum melt layer thickness for typical VDE conditions to be up to 3 mm [24]. However, this number should be considered as a conservative estimation. Experimental simulations with electron beams do not take the vapor shielding effect completely into account, since the highly energetic electrons can easily penetrate through the beryllium vapor and most of the energy is absorbed by the armor tile. Modelling without vapor shielding shows that a beryllium layer of about 7.5 µm is vaporized per VDE of 60 MJ m^{-2} over 100 ms [25]. This can be considered as an acceptable loss, since only a few to tens of VDEs are expected [26] for the lifetime of ITER. The vapor shielding effect [27] or other radiative cooling measures can significantly decrease the melt layer thickness and the amount of material lost during VDEs.

2.2. Disruptions, massive gas injections (MGIs), and shattered pellet injections (SPIs)

Plasma instabilities or e.g. a sudden cooling of the plasma by impurities can trigger a plasma current collapse (current quench), leading

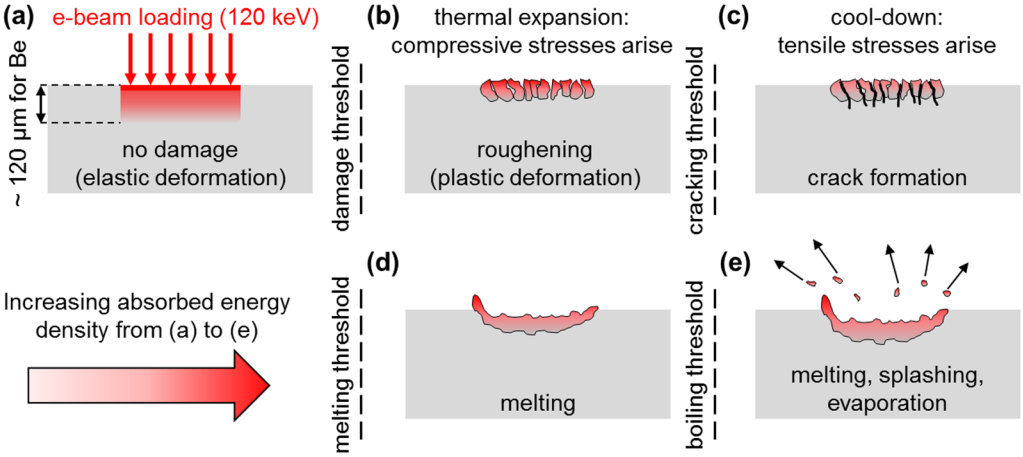

Fig. 1. Schematic view of the possibly induced damages during transient thermal loads. (a) Electron beam testing with loading conditions below the damage threshold, elastic deformation regime. (b) Damage threshold exceeded, plastic deformation occurs in the heat up phase due to compressive stresses in the loaded area that exceed the yield strength (locally and at the local temperature). (c) Cracking threshold exceeded, cracking occurs due to tensile stresses that exceed the ultimate tensile strength during/after cool down in the loaded area. (d) Melting threshold exceeded. (e) Further increase of the absorbed energy density can lead to evaporation/boiling and ejection/splashing of the molten material. Note that splashing can already occur below the boiling temperature due to rapid heating/expansion or electromagnetic forces.

to a plasma disruption and the subsequent deposition of the stored plasma energy (thermal quench) on the plasma facing components. The thermal energy of a full performance plasma in ITER is about 350 MJ. This energy will be deposited on a localized area in the divertor region and partially on the first wall, leading to melting and vaporization of the affected material. The potential damage of a single unmitigated disruption including mechanical stresses at the structural components by arising halo currents is too significant to allow for the continued safe operation of the machine. The massive injection of noble gases (MGI) with supersonic speeds or, more recently, shattered pellets (SPI) [28] have proven to be a simple and reliable method to mitigate the potential damage of plasma disruptions. Both techniques transform the thermal energy of the plasma into radiation energy in the millisecond time scale. Up to 1000 high energy plasma disruptions that have to be mitigated are expected for the lifetime of ITER [29].

If the stored energy of 350 MJ is homogeneously distributed over the plasma facing surface of about 830 m^2 [1], the resulting energy density would be around 0.42 MJ m^{-2}. However, due to local asymmetries of the photonic energy distribution, energy densities of up to 0.90–1.3 MJ m^{-2} are expected on the chamber walls [29]. Together with the expected plasma cooling times of 5–10 ms [29], this translates to heat flux factors of F_{HF} = 9–18 MW m^{-2} $s^{0.5}$. This is below the melting threshold of beryllium of F_{HF} = 23 MW m^{-2} $s^{0.5}$ at the expected base temperature of 523 K. Nevertheless, recent experiments with electron beam loading have shown that repetitive pulses with energy densities below the melting threshold successively decrease the thermal conductivity in the damaged layer and eventually lead to melting [30]. The melt layer thickness was about 80 μm after 1000 pulses with 1.3 MJ m^{-2} deposited over 5 ms (F_{HF} = 18 MW m^{-2} $s^{0.5}$, T_{base} = 523 K), while significant evaporation has not been observed. In the QSPA facility, a melt layer thickness of 10–20 μm [7] was observed for one pulse of 0.5 MJ m^{-2} deposited over 0.5 ms (F_{HF} = 22 MW m^{-2} $s^{0.5}$, T_{base} = 773 K). Furthermore, it was determined that the melt layer forms a hill and valley structure with a growth rate of 1 μm per pulse and no saturation up to 100 pulses was observed [29]. Based upon calculations, a radiation energy density of 1 MJ m^{-2} deposited over 1 ms (F_{HF} = 32 MW m^{-2} $s^{0.5}$, T_{base} not specified) resulted in a melt layer thickness of ~50 μm and an evaporated layer thickness of about ~10 μm [25], without taking vapor shielding into account. The total affected armor thickness for the highest expected MGI loads was ~340 μm over the lifetime of ITER [30].

Comparing the results obtained with different experimental loading methods simulating MGI characteristics (electron beam, photon flash through braking an argon-doped hydrogen plasma) shows that the methods yield significant differences in the melt/evaporation layer thickness and the induced surface morphology change. Electron beam experiments tend to overestimate the melt layer depth while possibly underestimating the evaporation layer due to the less steep thermal gradient and lower maximum surface temperature for a given heat load due to the significant electron penetration depth and consequent volumetric heating. The near-surface photonic loading method in the QSPA facility is closer to MGI characteristic loading. However, the full parameter space of absorbed energy densities and expected number of high energetic MGIs at the foreseen base temperature of beryllium of about 523 K has yet to be explored.

2.3. Runaway electrons

Under certain conditions, electrons circulating in the plasma can be accelerated to relativistic speeds with energies of several to tens of MeV. An extensive review about the emergence, physics basis, and implications of runaway electrons (REs) for the safe operation of ITER is presented in [31]. The low probability of this kind of event – around one in a thousand plasma discharges – makes it delicate to perform dedicated RE experiments in currently operating fusion devices. Nevertheless, the impact area on the main chamber wall of such a relativistic electron beam is more confined compared to disruption loads and the potential damage to the armor material and the heat sink is substantial. Such a beam is capable of deeply penetrating and melting any known material. Thus, the suppression of the formation of such a beam is a vital prerequisite to prevent prolonged maintenance periods in ITER.

In the unmitigated case, an RE beam can deposit 50 MJ m^{-2} over 300 ms on the FW modules resulting in a melt layer thickness of ~1.8 mm and a temperature of up to ~913 K at the beryllium-heat sink interface [32]. Once an RE beam has formed, it is difficult to mitigate it with the MGI technique due to the low coupling of the cold background plasma to the RE beam, which inhibits neutral particles from reaching the core of the beam [33]. In contrast, SPI as technique to suppress the formation of REs and to dissipate already formed beams is more promising, since the pellets can be injected directly into the RE beam [34]. Overall, the implications of REs for the beryllium armor fall into the same category as disruptions. Direct contact will lead to deep melting and potential damage of the heat sink, while the mitigation techniques lead to a much more homogeneous distribution of the energy, causing roughening and/or melting up to few tens of μm at most.

2.4. Edge localized modes

Up to this date, only a few experimental observations and simulations that allow a rough forecast to which extent edge localized modes (ELMs) will affect the main chamber wall in ITER are available. For example, in ASDEX Upgrade it has been found that up to 25% of the plasma energy loss for Type-I ELMs is deposited in non-divertor regions [35]. For the ITER divertor, power fluxes of up to 1 GWm^{-2} for durations of 0.2–0.5 ms (F_{HF} = 14–22 MW m^{-2} $s^{0.5}$) are expected during mitigated Type-1 ELMs [36]. Accordingly, as a conservative conjecture, fluxes with comparable characteristics can impact the FW.

During high confinement mode operation, ELMs occur with a frequency of several Hz, while mitigation techniques can increase the frequency to several tens of Hz, leading to pulse numbers greater than 10^7 over the operating time of ITER. Important factors to keep in mind are firstly, as mentioned in Section 2.2, the FW covers a considerably larger plasma facing surface area than the divertor. Secondly, it is unlikely that each particular ELM filament is affecting the same surface area on the FW. Hence, the number of ELM pulses that affects a given area on the FW is reduced by an unknown factor. A fluid model simulation of controlled ELMs in ITER with $\Delta W_{ELM} \approx 0.6$ MJ and f_{ELM} = 67 Hz using probability functions for ELM filament characteristics obtained in MAST and ASDEX Upgrade was performed in [37]. The power deposition profile had a total length of ~80 μs and a maximum power density of ~0.6 GWm^{-2} peaking at ~20 μs. This profile yields a heat flux factor of approximately $F_{HF} \approx 4$ MW m^{-2} $s^{0.5}$, calculated for a rectangular temporal pulse shape with a duration of 40 μs at the peak power density. An experiment applying thermal loads with comparable characteristics to S-65 beryllium samples is presented in [38]. Thereby, it was found that the inflicted damage saturated between 10^4 and 10^6 pulses as long as the applied heat flux factor remained at or below $F_{HF} \approx 9$ MW m^{-2} $s^{0.5}$. More details from this test campaign will be given in Section 3.

3. Combined transient thermal load results

In this section, an overview and key results of transient thermal loading experiments on beryllium carried out over the past five years at Forschungszentrum Jülich (FZJ) is presented. The dependency of surface modifications on the absorbed power density and base temperature has been examined in [39]. Thereby, it has been determined that a low base temperature is favorable for less severe surface modifications. This result is expected since both the yield strength and the ultimate tensile strength of S-65 beryllium decrease with increasing temperature and accordingly the material resistance to thermally induced stresses. These

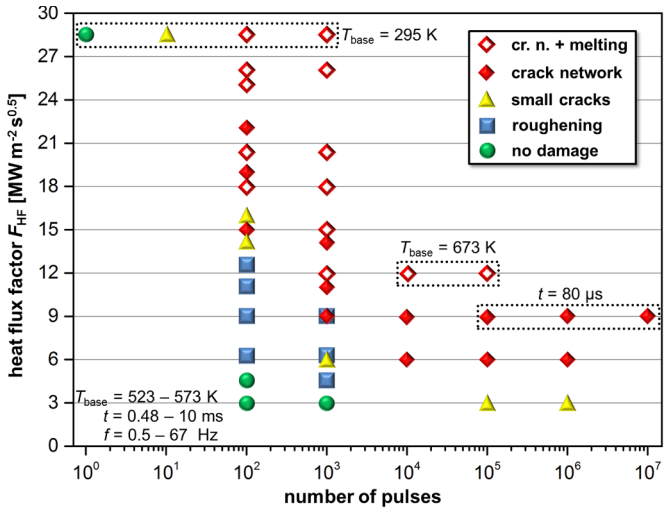

Fig. 2. Overview of transient thermal load testing performed in JUDITH 1 (1–10^3 pulses) and JUDITH 2 (10^4–10^7 pulses). The worst damage found on the loaded area defined the damage category (symbol/color code). If not specified otherwise, the loading conditions in the bottom left corner apply. (For interpretation of the references to color in this figure legend, the reader is referred to the web version of this article.)

results among others from [30,38,40] are illustrated in Fig. 2 in dependence on the applied heat flux factor and pulse number. An FEM simulation was performed in order to confirm that the comparison of transient thermal loads with a rectangular temporal pulse shape and pulse durations between 0.08 ms and 10 ms via the heat flux factor is reasonable. As a result, for F_{HF} = 9 MW m^{-2} s$^{0.5}$ with t_1 = 0.08 ms and t_2 = 10 ms, the temperature rise difference at the end of the two pulses with different durations is less than 1%. For comparison, the differences from t_1 to t_3 = 20 ms and t_4 = 100 ms are 2% and 19%, respectively. Furthermore, a dependency of the transient temperature profile on the pulse frequencies in the range of f = 0.5–67 Hz has not been found [38].

The upmost data points in Fig. 2 are from samples that were loaded with $F_{HF} \approx$ 28.5 MW m^{-2} s$^{0.5}$ at room temperature. The calculated peak temperature, factoring in the electron penetration depth, for this loading condition is T_{max} = 1329 K, well below the melting temperature of beryllium of 1560 K. However, as it can be seen in Fig. 2, fatigue effects quickly deteriorate the surface condition up to the point where molten areas could be identified in the loaded area after 10^2 pulses. The trend of a deteriorating surface condition for increasing pulse numbers holds true for all applied heat flux factor levels.

Even for the lowest heat flux factor that was technically achievable in the JUDITH 2 facility, it could be shown that no visible surface damage can turn into a roughened surface with small cracks if the applied pulse number is large enough, as it can be seen in Fig. 3. This result also

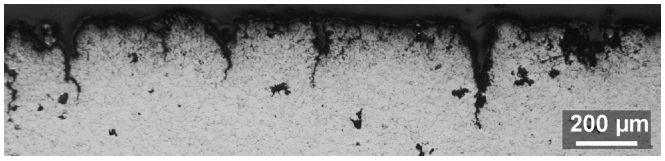

Fig. 4. Light microscopy image of the cross section of an S-65 beryllium sample loaded with 10^7 pulses of F_{HF} = 9 MW m^{-2} s$^{0.5}$ with t = 0.08 ms at T_{base} = 523 K. The peak temperature for a typical pulse was T_{max} = 993 K, measured by a single color fast pyrometer with the assumed emissivity ε = 0.1 (based on calibration and literature data). Note that the value of T_{max} is close to the analytically calculated value of 949 K, indicating that the assumed emissivity value is reasonable. The exact emissivity value depends on the surface condition at any given pulse and is therefore difficult to obtain.

indicates that during thermal loading with relatively mild conditions, material defects and mechanical stresses are induced, which accumulate with an increasing number of pulses, as it has been observed in tungsten [41]. The experiment in [38] identified the range of $F_{HF} \approx$ 9–12 MW m^{-2} s$^{0.5}$ to be the threshold between the saturation of induced damage and the consecutive destruction of the material with each pulse.

A cross section of the area loaded with F_{HF} = 9 MW m^{-2} s$^{0.5}$ and 10^7 pulses, the highest number of pulses which has been experimentally tested so far, is displayed in Fig. 4. The deepest measured crack in the loaded area extended down to 350 µm below the original surface. Such deep cracks were rare. Most of the damage was limited to the first ~100 µm below the surface. Given the fact that the applied heat flux factor was about two times higher than the predicted load from ELM filaments in [37], it can be expected that the heat loads coming from ELMs do not contribute significantly to the erosion of beryllium wall material in ITER. However, one has to keep in mind that microscopic damage in the form of dislocations or vacancies offers preferential sites for fuel retention. In addition, the refinement of the microstructure that is visible in the cross section close to the surface in Fig. 4 with an increase in the grain boundary density could also affect the fuel retention characteristics. Dedicated fuel retention studies with similarly damaged beryllium are required to obtain a more profound understanding of the implications of the thermally induced damage on plasma surface interaction relevant properties.

3.1. Oxidation effects

During the thermal shock loading experiments summarized above, it became evident that both the surface and intrinsic oxidation behavior of beryllium are influenced by the loading. Surface oxidation due to transient thermal loads is covered in [42]. It has been found that the thermally induced stresses accelerate the formation of oxide particles up to a significantly faster rate compared to simple holding at the peak temperature of the transient thermal load. The tests in [42] were conducted at a maximum oxygen partial pressure of 2×10^{-5} mbar.

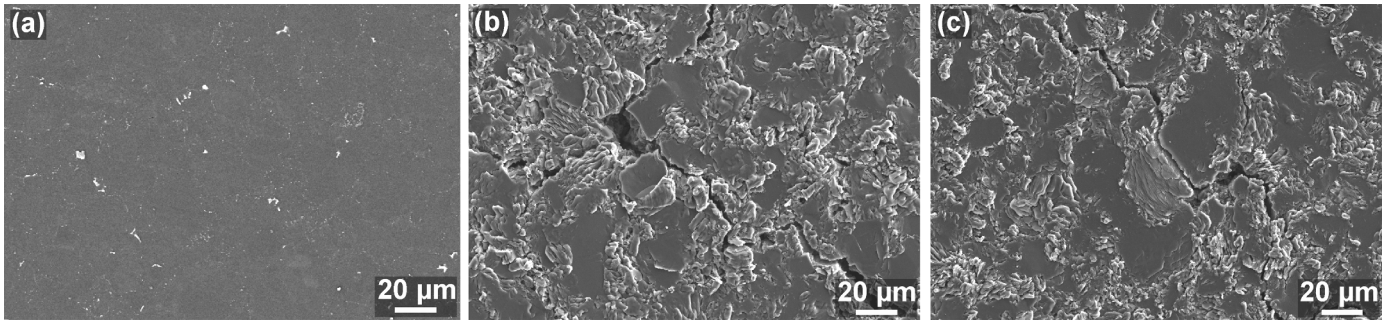

Fig. 3. Scanning electron microscopy images of S-65 beryllium samples loaded in JUDITH 1 (a) and JUDITH 2 (b), (c) with F_{HF} = 3 MW m^{-2} s$^{0.5}$ at T_{base} = 523 K with different numbers of pulses. (a) 10^3 pulses, no visible damage. (b) 10^5 pulses, small cracks. (c) 10^6 pulses, small cracks.

Experiments at lower/varying oxygen partial pressures are suggested to study the behavior in more detail. In current machines like JET it was determined that beryllium oxide is also present in co-deposited layers on divertor tiles [43]. These findings underline the relevance of beryllium oxide and its influence on operation sensitive characteristics, e.g. mixed material formation, fuel retention, erosion yield, etc.

The behavior of the intrinsic beryllium oxide in the bulk material is discussed in [44]. The loading with MGI- and ELM-relevant parameters resulted in the segregation of oxygen towards the grain boundaries up to a depth of ~120 μm if the maximum temperature during the loading exceeded T_{max} = 1209 K after already 10^2 pulses. This oxide segregation decreased the thermal conductivity of the affected layer and for loading conditions that caused melting, a reduced cohesion of the melt layer to the bulk material was observed. It was concluded that the oxide segregation is a time and temperature dependent process and could take place at lower values for T_{max} during the loading if the pulse number, i.e. holding time, is increased. The loading conditions for the sample displayed in Fig. 4 (F_{HF} = 9 MW m^{-2} s$^{0.5}$, t = 0.08 ms, T_{base} = 523 K, T_{max} = 993 K, 10^7 pulses) did not lead to the formation of a distinct oxide segregation layer in a certain depth, even though 10^7 pulses and an accordingly significantly higher holding time at elevated temperatures was applied. However, it can be seen that the grain boundaries close to the surface appear darker compared to those in a few hundred μm depth, which indicates that they have been more strongly etched by the cross section preparation. A stronger etching effect is observed when more oxygen is present at the respective location. Hence, also for these testing conditions the migration of oxygen to the grain boundaries is assumed. Nevertheless, the effect on the thermal conductivity seems to be minor in this case, since the damage in the loaded area saturated and the measured peak temperature did not significantly increase throughout the loading. Overall, the present results indicate that the transition region formation in a depth of ~120 μm in [44] is more related to the electron penetration depth (JUDITH 1: ~120 μm, JUDITH 2: ~18 μm) than to the pure thermal effects, at least for ELM-like loading conditions. It has yet to be confirmed if the oxide segregation has a considerable effect for MGI-like loading applied by a near-surface loading method, excluding the electron penetration depth effect.

3.2. Neutron effects

The in-vessel components in ITER will be exposed to high energetic neutrons that are generated in fusion reactions mostly during the DT phase. Thus, the effect of neutron irradiation with relevant fluences on the performance of the plasma facing components needs to be investigated in terms of mechanical properties, thermal properties, and steady state/transient high heat flux durability. Due to the unavailability of powerful neutron sources with a fusion relevant energy spectrum (strong peak at ~14 MeV), material specimens and components of interest are subjected to neutrons coming from fission sources with energies of ≲2.5 MeV [45].

One of the responses of beryllium to neutron irradiation is swelling due to the nuclear reaction of beryllium to helium and the subsequent formation of helium bubbles in the material. Swelling does not exceed 0.1% after neutron irradiation with a fluence of 5.5 × 10^{25} m^{-2} at 923–973 K base temperature [46]. Furthermore, the ultimate tensile strength and yield strength of S-65 grade beryllium decrease by ~30% at the same irradiation conditions, determined by tensile tests at room temperature. The thermal conductivity of beryllium decreases by ~20% after irradiation at 473 K base temperature with a neutron fluence of 3.8 × 10^{25} m^{-2} [47], which translates to approximately 1.5 dpa (displacements per atom) for beryllium, the expected lifetime dose of the FW armor tiles in ITER [48]. The irradiation generates dislocation loops and helium bubbles in beryllium, which act as additional points of phonon and electron scattering in the lattice and thereby decrease the thermal conductivity. Higher base temperatures during neutron irradiation tend to lead to a lower decrease of the thermal conductivity due to the thermal annealing of the neutron induced defects.

Furthermore, it has been reported that the erosion yield of irradiated beryllium increases by a factor of 1.5–2.5 [49]. This effect can be attributed to both the increasing temperature during the loading with the same loading conditions and the neutron induced embrittlement [50], which leads to more cracking and brittle destruction of the material during transient heating cycles. In summary, the performance of beryllium under transient thermal loads is likely to be adversely affected by neutron irradiation. However, considering the rather moderate total neutron fluence expected for the beryllium tiles in ITER, the negative effects on the affected armor thickness during transient loads remain limited.

4. Conclusions

With the scaling in size and stored plasma energy from currently operating tokamaks to ITER, new challenges arise regarding the damage potential of transient thermal loads and their mitigation. In this work, the effects of such transient loads on the FW armor material beryllium have been reviewed. VDEs without radiative cooling can cause a melt depth of ~3 mm but the cracking is confined to the melt layer and the connection of the melt to the bulk remains good for a few melt cycles. Unmitigated disruptions have similar effects on beryllium. Note that for unmitigated disruptions, most of the plasma energy is deposited localized in the divertor, which is the limiting component in this case. The number of unmitigated disruptions/VDEs has to be limited to a few events even for the FW modules, which typically see lower loads compared to the divertor, to prevent millimeter deep melting, splashing of armor material, and damage of the joint/heat sink material.

The MGI/SPI methods have proven to be effective mitigation methods for plasma disruptions. The drawback, however, is the significant thermal load that is spread via radiation to the entire FW, potentially causing cyclic melting of the beryllium armor tiles. If the observed trend of hill growth of 1 μm per MGI pulse does not saturate up to 1000 pulses, a pronounced hill-valley structure with height differences of about a millimeter would be the result. Electron beam tests with MGI/SPI loading conditions did not result in a pronounced hill-valley formation, which could be attributed to the more volumetric heating in contrast to the pure surface heating in the QSPA facility. The affected armor thickness has been determined to be ~340 μm for the highest expected MGI loads over the lifetime of ITER. This value could be affected by the electron penetration depth and needs to be confirmed with a near surface loading method, e.g. laser. The effect of melt motion could also play a significant role in the affected armor thickness and surface morphology change during operation.

The testing of beryllium under ELM-like loading conditions, as they were predicted with recent fluid model simulations, resulted in a maximum affected armor thickness of 350 μm for as much as 10^7 pulses. The threshold heat flux factor that would critically affect the FW is in the range of F_{HF} ≈ 9–12 MW m^{-2} s$^{0.5}$. However, if such heat loads from ELMs arrive at the FW, the according loads arriving at the divertor would be even greater. Hence, the resistance of the tungsten armor in the divertor against thermal loads coming from ELMs is most relevant for the overall machine durability. The available results suggest that the ELMs that are tolerable for the divertor pose no significant threat to the viability of the FW beryllium armor.

Neutron irradiation has a deteriorating effect on the thermo-mechanical properties of beryllium, which are the major influencing factors in determining the degree of the damage inflicted by transient thermal loads. The relatively low neutron fluence during the lifetime of ITER, compared to a DEMO (demonstration power plant) type reactor, reduces the beryllium material strength by some tens of percents. If the affected armor thickness from transient loads, which has been mostly obtained from non-irradiated testing so far, increases at a comparable

rate, the safety margin between the affected and total armor thickness remains sufficient.

It is not envisaged to replace or upgrade all of the FW modules during the service time of ITER, in contrast to the divertor, which is scheduled to be replaced after ~25,000 plasma discharges [51]. Thus, the beryllium armor must retain its full capabilities into the DT operational phase of ITER to enable the demonstration of the viability of fusion as energy source. Based on the present review, the thermal loads arising through MGIs/SPIs on the beryllium armor tiles are expected to be the most relevant damaging factor.

Acknowledgments

The authors would like to kindly thank G. Knauf for her benevolent assistance in the preparation of the samples and for the performance of the cross section microscopy as well as Dr. E. Wessel for capturing the scanning electron microscopy images.

References

[1] M. Merola, F. Escourbiac, et al., Fusion Eng. Des. 89 (7–8) (2014) 890–895.
[2] E. Bertolini, Fusion Eng. Des. 30 (1995) 53–66.
[3] G. Janeschitz, J. Nucl. Mater. 290–293 (2001) 1–11.
[4] G. Federici, et al., Fusion Eng. Des. 61–62 (2002) 81–94.
[5] R. Behrisch, et al., J. Nucl. Mater. 313–316 (2003) 388–392.
[6] R.P. Doerner, J. Nucl. Mater. 438 (2013) S272–S275.
[7] D.V. Kovalenko, Nuclear Mater. Energy 12 (2017) 156–163.
[8] G.F. Matthews, J. Nucl. Mater. 337–339 (2005) 1–9.
[9] S. Brezinsek, et al., J. Nucl. Mater. 463 (2015) 11–21.
[10] M. Gyoeroek, et al., J. Nucl. Mater. 472 (2016) 76–81.
[11] K. Sugiyama, et al., Nuclear Mater. Energy 6 (2016) 1–9.
[12] Y. Ueda, et al., Nucl. Fusion 57 (2017) 092006.
[13] J.H. Yu, et al., Phys. Scr. T167 (2016) 014033.
[14] J.H. Yu, et al., Nucl. Fusion 55 (2015) 093027.
[15] J. Linke, Trans. Fusion Sci. Technol. 49 (2006) 455–464.
[16] V. Barabash, et al., Phys. Scr. T145 (2011) 014007.
[17] M. Roedig, et al., J. Nucl. Mater. 417 (2011) 761–764.
[18] R. Duwe, et al., Fusion Technol. Proc. 1 (1995) 356–358.
[19] I.B. Kupriyanov, Fusion Eng. Des. 124 (2017) 1004–1010.
[20] H.-Y. Chen, et al., Fusion Eng. Des. 121 (2017) 130–136.
[21] A. Hassanein, J. Nucl. Mater. 438 (2013) S1266–S1270.
[22] X. Liu, J. Nucl. Mater. 442 (2013) S309–S312.
[23] V. Barabash, et al., Phys. Scr. T145 (2011) 014007.
[24] H. Bolt, et al., J. Nucl. Mater. 307–311 (2002) 43–52.
[25] G. Federici, Compr. Nucl. Mater. 4 (2012) 621–666.
[26] J. Linke, Fusion Sci. Technol. 46 (1) (2004) 1423–151 https://dx.doi.org/10.13182/FST04-A550.
[27] K. Ibano, et al., Nucl. Mater. Energy 12 (2017) 278–282.
[28] S. Pestchanyi, Fusion Eng. Des. 136(A) (2018) 29–33.
[29] N.S. Klimov, J. Nucl. Mater. 463 (2015) 61–65.
[30] B. Spilker, Nucl. Mater. Energy 9 (2016) 145–152.
[31] A.H. Boozer, Nucl. Fusion 57 (2017) 056018(14pp).
[32] A.R. Raffray, et al., B. Beaumont, et al. (Ed.), Proceedings of the 20th Symposium on Fusion Technology, Marseille, France, Vol. 1 1998, p. 211 1998.
[33] C. Reux, Nucl. Fusion 55 (2015) 093013(17pp).
[34] N. Commaux, Nucl. Fusion 56 (2016) 046007(7pp).
[35] A. Herrmann, et al., Plasma Phys. Control. Fusion 46 (2004) 971–979.
[36] M. Wirtz, Fusion Eng. Des. 88 (9–10) (2013) 1768–1772.
[37] M. Kočan, et al., J. Nucl. Mat. 463 (2015) 709–713.
[38] B. Spilker, Nucl. Mater. Energy 12 (2017) 1184–1188.
[39] B. Spilker, et al., Phys. Scr. T167 (2016) 014024(4pp).
[40] B. Spilker, Fusion Eng. Des. 109–111 (Part B) (2016) 1692–1696.
[41] W. Van Renterghem, et al., Nucl. Mater. Energy 9 (2016) 484–489.
[42] B. Spilker, et al., Phys. Scr. T170 (2017) 014055(6pp).
[43] M. Rubel, et al., Fusion Eng. Des. 136(A) (2018) 579–586.
[44] B. Spilker, Nucl. Fusion 56 (2016) 106014(9pp).
[45] M. Devlin, et al., Nucl. Data Sheets 148 (2018) 322–337.
[46] I.B. Kupriyanov, et al., Fusion Eng. Des. 51–52 (2000) 135–143.
[47] V. Chakin, et al., Prog. Nucl. Energy 57 (2012) 2–7.
[48] V. Barabash, et al., J. Nucl. Mater. 313–316 (2003) 42–51.
[49] M. Roedig, et al., J. Nucl. Mater. 283–287 (2000) 1161–1165.
[50] M. Roedig, et al., J. Nucl. Mater. 307–311 (1) (2002) 53–59.
[51] R.A. Pitts, et al., J. Nucl. Mater. 438 (2013) S48–S56.